Research Article Vol. 9, No. 7 / 1 July 2019 / Optical Materials Express 2785
Optical Materials EXPRESS

Effect of the residual doping on the performance of InN epilayers as saturable absorbers for ultrafast lasers at 1.55µm

L. Monroy,[1,*] M. Jiménez-Rodríguez,[1] P. Ruterana,[2] E. Monroy,[3] M. González-Herráez,[1] and F. B. Naranjo[1]

[1]Grupo de Ingeniería Fotónica, Departamento de Electrónica (EPS) Universidad de Alcalá, Campus Universitario 28871 Alcalá de Henares, Madrid, Spain
[2]CIMAP; UMR 6252, CNRS-ENSICAEN-CEA-UCBN, 14050 Caen, France
[3]Univ. Grenoble-Alpes, CEA, INAC-PHELIQS, 17 av. Des Martyrs, 38000 Grenoble, France
*Corresponding author: laura.monroy@uah.es

Abstract: We report on the improvement of performance of InN-based saturable absorbers in fiber lasers operating at 1.55 µm by reducing the residual doping, due to the lower Burstein-Moss effect. The improved tuning of the band-to-band transition with respect to the operation wavelength leads to an enhancement of nonlinear optical effects, resulting in 30 % of modulation depth. We introduce the development of an ultrafast mode-locked fiber laser using an improved InN-based saturable absorber that incorporates a buffer layer between the active layer and the substrate. The laser delivers output pulses with a temporal width of ~ 220 fs, a repetition rate of 5.25 MHz, and high-pulse energy of 5.8 nJ.

1. Introduction

The demand of ultrashort pulsed radiation sources has grown during the last decades due to their introduction in application fields such as micro-machining [1], terahertz generation and detection [2], spectroscopy and microscopy [3], or eye laser surgery [4]. The cornerstone of ultrafast optics is the passive mode-locked laser. In the case of fiber lasers, passive mode-locking can be implemented using nonlinear optical elements such as nonlinear polarization rotators [5], nonlinear amplifying loop mirrors [6], or saturable absorbers [7–16]. Saturable absorption is a nonlinear effect where the optical transmittance of the material nonlinearly increases when raising the pumping intensity. Mode-locked fiber lasers incorporating saturable absorbers have been widely investigated due to their fabrication simplicity, compactness, and capability to achieve extremely short pulses (in the order of fs) with enormous peak power (up to tens of kW) for a wide range of operation wavelengths. Among saturable absorbers, semiconductor saturable absorbers have demonstrated great efficiencies for mode-locking lasers as well as convenient implementations. In this setting, III-nitride semiconductors have emerged as attractive materials for saturable absorbers in the telecommunication C-band (1.53 – 1.57 µm) since they present high thermal and mechanical stability and enhanced third-order nonlinearity due to the asymmetry of their crystalline structure. Particularly, a saturable absorber for operation in the C-band based on InN has been recently demonstrated [17]. The interest of InN stems from the proximity of its room temperature band gap to 1.55 µm (≃ 0.8 eV). However, it must be kept in mind that the absorption band edge of InN depends on the residual doping, mainly due to the Burstein-Moss effect [18]. Doping levels higher than 10^{20} cm^{-3} shift the absorption edge beyond 1 eV, rendering this material useless as saturable absorber for the C-band.In this letter, we discuss the effect of the doping on the performance of InN layers used as saturable absorbers for ultrafast fiber lasers operating at 1.5 µm. The improved tuning of the semiconductor absorption band gap energy by

#365886 https://doi.org/10.1364/OME.9.002785
Journal © 2019 Received 23 Apr 2019; revised 23 May 2019; accepted 23 May 2019; published 4 Jun 2019

Optical Materials EXPRESS

reducing the residual doping enables the fabrication of fiber lasers delivering ultrashort pulses (~ 220 fs) with a peak power of 26.5 kW and pulse energy up to 5.8 nJ.

2. Material characterization

The structure under study consists of a 1-μm-thick InN thin film deposited on a 4− µm-thick GaN-on-sapphire template by plasma-assisted molecular beam epitaxy. Growth was performed at 450 °C, at a nitrogen-limited growth rate of 280 nm/h. To improve the structural quality of the InN layer, a heterostructure consisting of 11 periods of InN/$In_{0.7}GaN_{0.3}$ (4.5 nm/7 nm) was inserted between the substrate and the InN film (sample A). The reduction of the defect density with this kind of buffer structure was discussed in [19]. The performance of this material as saturable absorber is discussed in comparison with a similar InN thin film synthesized in similar conditions but grown directly on the GaN-template substrate (Sample B), which was previously used for ultrafast fiber laser fabrication [19].

Figs. 1(a) and (b) show 1 µm × 2 μm atomic force microscopy (AFM) images of samples A and B, respectively. Sample A presents smooth surface morphology with atomic terraces. In the case of sample B, pits are visible in the surface with a density around $2x10^8$ cm^{-2}. Such pits constitute surface terminations of extended defects [20,21,22], mostly threading dislocations [20] opening up to exhibit inverted pyramids limited by {10-11} facets as depicted in Fig. 1(b). As a result, the root-mean-square roughness measured in 2 µm × 2 μm images increases from around 0.5 nm for sample A to close to 2 nm for sample B. Dark field transmission electron microscopy (TEM) images of sample A [see Fig. 1(b)] show that the 11-period MQW placed between InN and the GaN template help to reduce the threading dislocation density, as introduced in [23].

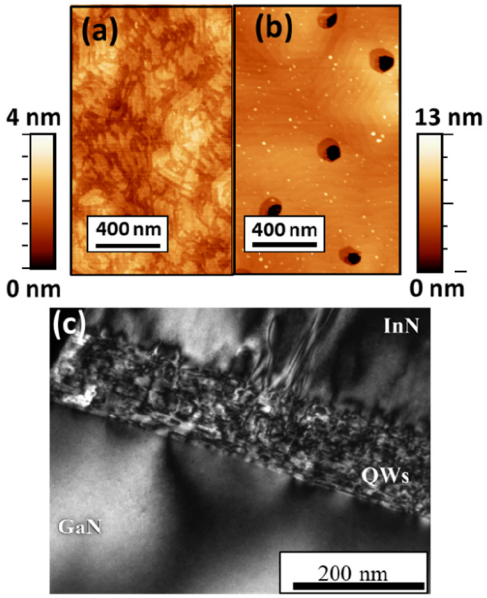

Fig. 1. AFM images of (a) sample A and (b) sample B. (c) Dark field TEM image showing the InN/InGaN MQW, between the InN layer and GaN template. Dark areas in the image correspond to the barriers, and brighter areas to the InN layers.

Optical transmittance spectra, shown in the inset of Fig. 2, have been measured using a white lamp as radiation source and an optical spectrum analyzer (OSA). Figure 2 depicts the Tauc plot [24] for each sample (thick line for sample A; thin line for sample B), plotting $(\alpha E)^2$ as a function of the incident radiation energy, E, where α is the linear absorption coefficient, which has been

Optical Materials EXPRESS

calculated using the following expression, $\alpha = -\ln[T(\lambda)]/l$, where $T(\lambda)$ is the transmittance spectrum and l is the layer thickness. The band gap energies estimated from the Tauc plots are ~ 0.77 eV and ~ 0.8 eV for samples A and B, respectively. The shift is explained by the different residual doping density, estimated to $4 - 5x10^{18}cm^{-3}$ for sample A, and over 10^{19} cm^{-3} for sample B. These values have been calculated from band gap energies and using the curve presented by J. Wu *et al.* [18]. The linear absorption at 1.55 μm is $\alpha_0 = 2\ x10^4 cm^{-1}$ for sample A and $\alpha_0 = 1.4\ x10^4 cm^{-1}$ for sample B, i.e. lowering the residual doping red shifts the band gap approaching it to the 1.55 µm operation wavelength, which results in an enhancement of the linear absorption.

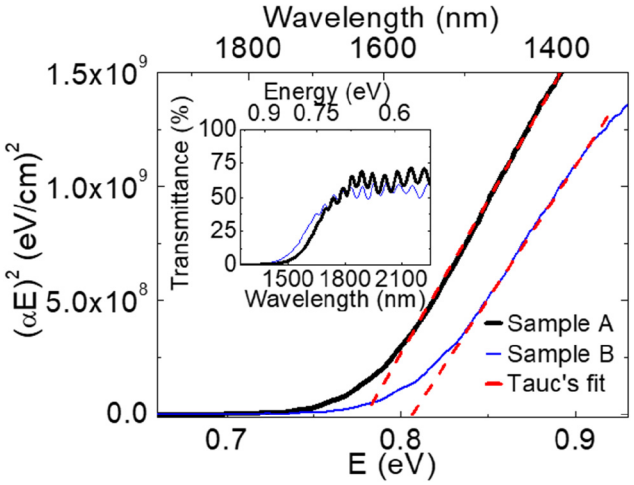

Fig. 2. Illustration of $(\alpha E)^2$ versus E for sample A (black thick line) and sample B (blue thin line). Red dashed line represents the Tauc's approximation. Inset: Linear transmittance measurements of each sample.

Nonlinear transmission measurements of the samples have been performed by applying the Z-scan technique, using an ultrafast fiber laser delivering pulses with a time width of 250 fs and maximum peak power of ~ 40 kW. A fiber collimator sends the optical pulse through the material under study, which is placed on a translation stage. At the output it is measured the transmission of the sample as a function of its position. In order to collect the maximum optical power onto the sample, a 3-cm lens is used in the experimental scheme. Thus, a knife-edge technique has been applied to characterize the incident beam employed for the nonlinear measurements [25,26], extracting a beam radius $\omega_0 = 8.5$ µm and a Rayleigh distance $z_R = 223.2$ µm.

Figure 3 presents the maximum transmission at the focal point obtained from the Z-scan transmission measurements [27] when varying the optical fluence of the laser pulse. In order to extract the nonlinear parameters of the layers, the experimental data are fitted to [17]:

$$T = T_{ns}\frac{\ln(1 + T_{lin}\Big/ T_{ns}(e^{F/F_{sat}} - 1))}{F/F_{sat}} \tag{4}$$

where T_{lin} and T_{ns} are the linear and non-saturable transmittance, respectively, F is the fluence, calculated taking into account the beam radius estimated previously, and F_{sat} the saturation fluence. For sample A, we find $F_{sat} = 1015 \pm 45\mu J/cm^2$, $T_{lin} = 13 \pm 1\%$ and $T_{ns} = 40 \pm 4\%$. These results imply a maximum modulation depth (estimated as $\Delta T = T_{ns} - T_{lin}$) around 27%. Sample B, on the other hand, presents $F_{sat} = 990 \pm 30\mu J/cm^2$, $T_{lin} = 28 \pm 3\%$ and $T_{ns} = 45 \pm 5\%$, which implies a maximum modulation depth around $\Delta T = 17\%$. Furthermore, both samples have proved to support fluence above 12 mJ/cm^2 without apparent optical damage.

Optical Materials EXPRESS

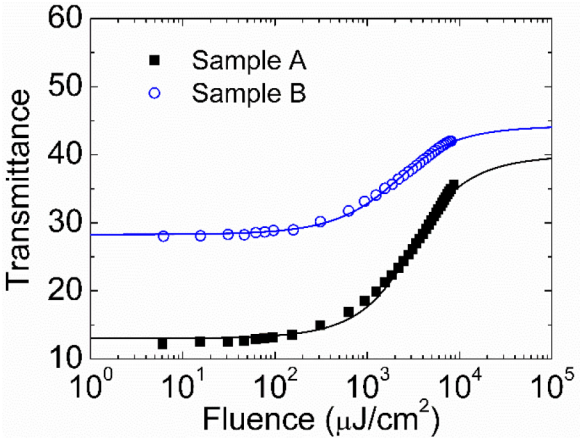

Fig. 3. Optical transmittance as a function of the impinging fluence of samples A and B. Solid lines are fits to Eq. (4).

In relation to the results obtained in previous works [17], due to the introduction of the heterostructure between the InN film and the substrate, and considering a similar saturation fluence between the samples, it has been achieved a higher modulation depth of sample A in comparison to sample B. This change in the modulation depth is attributed to the considerable reduction of the linear transmission of the sample, which implies an increment in the material efficiency. As a consequence, a higher nonlinear response in the material is obtained and therefore a larger optical power at the output. Considering these features, sample A can be considered an adequate candidate for the implementation as a saturable absorber for the generation of ultrafast laser sources.

3. Laser properties

To assess the performance of sample A as saturable absorber, the sample was placed inside a fiber ring laser cavity. The components of the laser resonator were as in [17], namely a commercial Er-doped fiber amplifier (EDFA) with up to 24 dBm output power as gain medium (Accelink, TV Series), a variable optical attenuator, to control the losses in the cavity, and an optical fiber coupler, resulting in a total ~40m cavity. The saturable absorber was placed in a free space region in a transmission configuration (Fig. 4), between two 3-cm-focal achromatic lenses, to increase the fluence that impinges the material, and a collimator and microscope objective were used to launch and collect the light respectively between the optical fiber and free space. In this work, we used a 70/30 fiber coupler, i.e. 70 % of the light is recirculated in the ring resonator, while the remaining 30 % is launched as laser output. Additionally, two 99/1 fiber couplers were set in cascade at the laser output, in order to monitor simultaneously the average power, using an InGaAs-based power meter (Thorlabs, PM100USB), the optical spectrum using the above-described OSA, and the autocorrelation trace (APE-Mini autocorrelator).

The laser cavity behaves as a dispersion-managed cavity, whose net dispersion coefficient is estimated at -0.26 ps^2. Therefore, the laser operates in the anomalous dispersion regime. The mode-locking operation of the laser is self-starting, being triggered when a certain average power threshold is reached. Further details and discussion about the cavity design and dispersion properties can be found in [17]. The laser exhibits a repetition rate of 5.25 MHz, which was measured using an electrical spectrum analyzer (Agilent Technologies, model N9010A). According to this value of repetition rate, which coincides with the one expected from the cavity length of the experimental laser set-up, no higher-order harmonics have been visualized.

Optical Materials EXPRESS

When operating in mode-locking regime, the peak-to-noise ratio from the ESA measurement (Fig. 5) is estimated over 45 dB, limited by the maximum dynamic range of the balanced detector (PDB410CAC, Thorlabs).

Using sample A as saturable absorber, an analysis of the variation of the laser properties as a function of the power inside the cavity (i.e., the energy applied to the saturable absorber) was performed. For these measurements, the average power was varied using the variable attenuator while keeping the EDFA delivering the maximum possible output power. The laser enters the mode-locking regime of operation when the output average power is higher than 21 mW. The maximum average output power obtained is 30.6 mW when the variable attenuator is fully opened. Figures 6(a) and (b) show the autocorrelation function (measured from a commercial autocorrelator APE Mini) and spectrum (measured using an optical spectrum analyzer, Yokogawa AQ-6315B) of the laser output, respectively, in the particular case of minimum attenuation (average output power = 30.6 mW). The pulse width is $\Delta\tau$ = 220 fs and the spectral width is $\Delta\lambda$ = 21.8 nm (extracted from the full-width at half maximum of the Sech^2 fits presented in the figures). Note that the spectra do not display Kelly sidebands, which is a common feature in strong dispersion managed cavities [28]. In the range of mode-locking operation, the pulse duration increases up to $\Delta\tau$ = 235 fs (spectral width decreasing to $\Delta\lambda$ = 17.6 nm when decreasing the average output power to 21 mW (onset of mode-locking regime). From these values, the peak power has been found to scale from 18 kW to 26.5 kW as a function of the average output power, as shown in the left axis of Fig. 6(c), corresponding to the pulse energy varying from 4.3 nJ to 5.8 nJ. Moreover, the right axis of Fig. 6(c) depicts the estimated time-bandwidth product (TBP), which oscillates from 0.354 to 0.407 (TBP limit for Sech^2 pulses is 0.315), indicating that the pulses are slightly chirped.

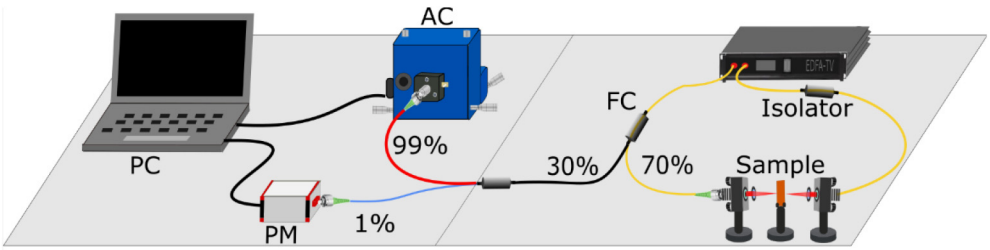

Fig. 4. Laser set-up: the laser cavity consists on a EDFA amplifier that after interacting with the semiconductor saturable absorber in a free-space transmission configuration, delivers a 220fs pulse. The output optical power and temporal duration are monitorized by a power meter (PM) and an autocorrelator (AC).

Regarding sample B, Fig. 6(b) shows in green dashed line the spectrum obtained using this material with the 70/30 fiber coupler. With this sample, it was not possible to achieve stable mode-locking, being only possible to reach a transition range where continuous wave and mode-locking regimes coexist. This behavior can be explained in terms of the larger linear absorption of sample A, with respect to sample B, taking into account that the InN layer has the same length for both cases. The larger absorption hinders the propagation of the continuous wave and forces the saturable absorber to work under nonlinear regime, thus maintaining the mode-locked operation. On the other hand, for sample B it was only possible to achieve stable mode-locking operation using a 90/10 fiber coupler, delivering pulses as short as $\sim$ 250 fs with maximum peak power achieved of 7.95 kW and pulse energy of 2 nJ. Note that the shorter pulses obtained for sample A can be explained in terms of the higher modulation depth shown by sample A, as explained by H. A. Haus [29]. Considering the operation wavelength and the maximum

Optical Materials EXPRESS

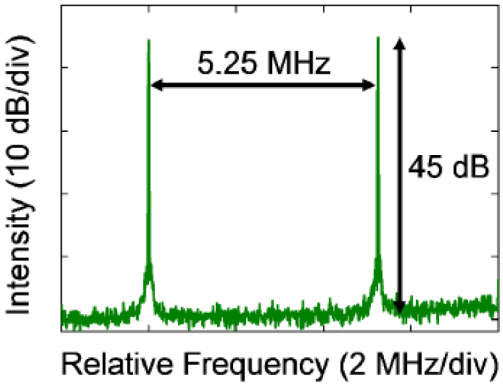

Fig. 5. Electrical spectrum of the detected pulse train with a repetition rate of 5.25 MHz, which corresponds to 190 ns separation between consecutive pulses.

intensity on the samples, it is expected that both samples are acting as slow saturable absorbers with a time response in the range of ps [19, 30].

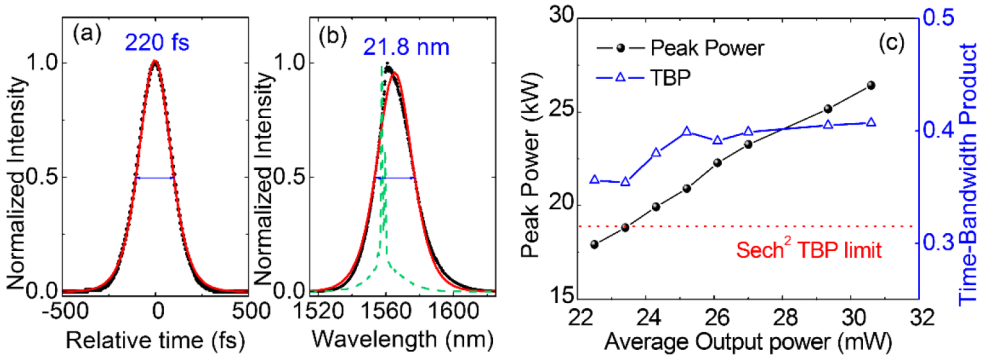

Fig. 6. Typical laser output using sample A at 30.6 mW output average power, showing: (a) autocorrelation function of the pulse, and (b) linear optical spectrum. Green dashed line corresponds to the spectrum for sample B using a 70/30 fiber coupler. Both traces have been fitted to a sech^2 pulse profile (red line) (c) Laser analysis in the mode-locking range of the laser as a function of the average output power, presenting the estimated peak power and the time-bandwidth product.

When comparing the two samples, there is a 3-fold improvement in terms of peak power and pulse energy by using sample A instead of sample B. This can be explained by the reduction of the residual doping effect generated between the two layers of InN and GaN during its growth process. As a consequence, the optical losses of sample A has been reduced in comparison to previous data, leading to pulses with higher optical powers.

At the maximum average output power (30.6 mW, when the variable attenuator is fully open) the optical power inside the cavity is higher than 70 mW, which implies that a fluence above 9 mJ/cm^2 impinges the InN layer, considering the knife-edge results. Even under these very high fluences, InN does not exhibit any sign of optical damage. This implies that InN is more suitable for high-energy applications than commonly used materials operating at 1.5 μm, as for example semiconductor-based saturable absorbers of InGaAs with a limited bandwidth operation [9], graphene, which has an ultra-broadband absorption property but has a low modulation depth [10,11], carbon nanotubes, whose bandwidth depends on the diameter of the nanotube and has

Optical Materials EXPRESS

high non-saturable losses [12], topological insulators, characterized by their broadband saturable absorption but still with a low modulation depth [13], transition metal dichalcogenides, whose optical properties depend on the established layers and are limited in the 1-2 eV energy bandgap [14] or black phosphorus, a very recent saturable absorber with a controllable direct bandgap, but still with some limitations such as its low modulation depth and its polarization dependence [15,16] among others. In general, these materials present damage thresholds lower than 2 mJ/cm^2, therefore limiting the output optical power. Furthermore, the lasers developed using InN-based saturable absorbers have proved to be polarization independent, since they do not require any element to control the polarization within the resonator. This feature is a clear advantage over fiber lasers using nonlinear polarization-rotators [5], nonlinear amplifying mirrors [6], or even many semiconductor-based saturable absorbers.

4. Conclusions

In conclusion, we report the variation of the performance of InN saturable absorbers as a function of the residual doping. Reduced residual doping results in larger nonlinear change in transmittance at 1.55 µm, attaining a modulation depth larger than 30 %. Inserting such InN layers in a laser resonator for mode-locked operation, we demonstrate ultrashort pulses of ~ 220 fs, with 26.5 kW peak power, and high-pulse energy of 5.8 nJ. This implies a 3-fold improvement in terms of peak power and pulse energy with respect to the latest reports [17].

Funding

Comunidad de Madrid (S2018/NMT-4326); Ministerio de Economía, Industria y Competitividad, Gobierno de España (TEC2015-71127-C2-2-R); Ministerio de Ciencia, Innovación y Universidades (RTI2018-097957-B-C31).

References

1. L. Shah, E. Fermann, J. W. Dawson, and C. P. J. Barty, "Micromachining with a 50W, 50µJ, sub-picosecond fiber laser system," Opt. Express **14**(25), 12546–12551 (2006).
2. M. Nagai and K. Tanaka, "generation and detection of terahertz radiation by electro-optical process in GaAs using 1.56 µm fiber laser pulses," Appl. Phys. Lett. **85**(18), 3974–3976 (2004).
3. H. N. Paulsen, K. M. Hilligsøe, J. Thøgersen, S. R. Keiding, and J. J. Larsen, "Coherent anit-Stokes Raman scattering microscopy with a photonic crystal fiber based light source," Opt. Lett. **28**(13), 1123–1125 (2003).
4. L. He, K. Sheehy, and W. Culbertson, "Femtosecond laser-assisted cataract surgery: three-month follow-up," Curr. Opin. Ophthalmol. **22**(1), 43–52 (2010).
5. X. M. Liua, T. Wanga, C. Shub, L. R. Wanga, A. Lina, K. Q. Lua, T. Y. Zhanga, and W. Zhao, "Passively harmonic mode-locked erbium-doped fiber soliton laser with a nonlinear polarization rotation," Laser Phys. **18**(11), 1357–1361 (2008).
6. A. V. Avdokhin, S. V. Popov, and J. R. Taylor, "Totally fiber integrated, figure-of-eight, femtosecond source at 1065 nm," Opt. Express **11**(3), 265–269 (2003).
7. E. Garmre and A. Yariv, "Laser mode-locking with saturable absorbers," IEEE J. Quantum Electron. **3**(6), 222–226 (1967).
8. R. I. Woodward and E. J. R. Kelleher, "2D saturable absorbers for fibre lasers," Appl. Sci. **5**(4), 1440–1456 (2015).
9. P. H. Hanzard, *et al.*, "Dissipative soliton laser mode-locked with a resonant InGaAs-based saturable absorber mirror," IEEE Photonics Technol. Lett. **29**(21), 1772–1775 (2017).
10. V. Mamidala, R. I. Woodward, Y. Yang, H. H. Liu, and K. K. Chow, "Graphene-based passively mode-locked bidirectional fiber ring laser," Opt. Express **22**(4), 4539–4546 (2014).
11. Z. Sun, T. Hasan, F. Torrisi, D. Popa, G. Privitera, F. Wang, F. Bonaccorso, D. M. Basko, and A. C. Ferrari, "Graphene mode-locked ultrafast laser," ACS Nano **4**(2), 803–810 (2010).
12. S. Y. Set, H. Yaguchi, Y. Tanaka, and M. Jablonski, "Laser mode locking using a saturable absorber incorporating carbon nanotubes," J. Lightwave Technol. **22**(1), 51–56 (2004).
13. P. Yan, R. Lin, S. Ruan, A. Liu, H. Chen, Y. Zheng, S. Chen, C.-Y. Guo, and J. Hu, "A practical topological insulator saturable absorber for mode-locked fiber laser," Sci. Rep. **5**(1), 8690 (2015).
14. J. Koo, J. Park, J. Lee, Y. M. Jhon, and J. H. Lee, "Femtosecond harmonic mode-locking of a fiber laser at 3.27 GHz using a bulk-like, $MoSe_2$-based saturable absorber," Opt. Express **24**(10), 10575–10589 (2016).
15. J. Sotor, G. Sobon, M. Wojciech, P. Pałetko, and K. Abramski, "Black phosphorus saturable absorber for ultrashort pulse generation," Appl. Phys. Lett. **107**(5), 051108 (2015).

Optical Materials EXPRESS

16. M. Zhang, Q. Wu, F. Zhang, L. Chen, X. Jin, Y. Hu, Z. Zheng, and H. Zhang, "2D Black Phosphorus Saturable Absorbers for Ultrafast Photonics," Adv. Opt. Mater. **7**(1), 1800224 (2019).
17. M. Jiménez-Rodríguez, L. Monteagudo-Lerma, E. Monroy, M. González-Herráez, and F. B. Naranjo, "Widely power-tunable polarization-independent ultrafast mode-locked fiber laser using bulk InN as saturable absorber," Opt. Express **25**(5), 5366–5375 (2017).
18. J. Wu, W. Walukiewicz, S. X. Li, R. Armitage, J. C. Ho, E. R. Weber, E. E. Haller, H. Lu, W. J. Schaff, A. Barcz, and R. Jakiela, "effects of electron concentration on the optical absorption edge of InN," Appl. Phys. Lett. **84**(15), 2805–2807 (2004).
19. S. Valdueza-Felip, L. Rigutti, F. B. Naranjo, P. Ruterana, J. Mangeney, F. H. Julien, M. González-Herráez, and E. Monroy, "Carrier localization in InN/InGaN multiple-quantum well with high In-content," Appl. Phys. Lett. **101**(6), 062109 (2012).
20. V. Potin, P. Ruterana, G. Nouet, R.C. Pond, and H. Morkoç, "Mosaic growth of GaN on (0001) sapphire: A high-resolution electron microscopy and crystallographic study of threading dislocations from low-angle to high-angle grain boundaries," Phys. Rev. B **61**(8), 5587–5599 (2000).
21. P. Ruterana, B. Barbaray, A. Béré, P. Vermaut, A. Hairie, E. Paumier, G. Nouet, A. Salvador, A. Botchkarev, and H. Morkoc, "Formation mechanism and relative stability of the $\{112^{-}0\}$ stacking fault atomic configurations in wurtzite (Al, Ga, In) nitrides," Phys. Rev. B **59**(24), 15917–15925 (1999).
22. P. Ruterana, V. Potin, B. Barbaray, and G. Nouet, "Growth defects in GaN layers on top of (0001) sapphire: A geometrical investigation of the misfit effect," Philos. Mag. A **80**(4), 937–954 (2000).
23. P. Ruterana, A. L. Syrkin, E. Monroy, E. Valcheva, and K. Kirilov, "The microstructure and properties of InN layers," Phys. Status Solidi C **7**(5), 1301–1304 (2010).
24. J. Tauc, "Optical properties and electronic structure of amorphous Ge and Si," Mater. Res. Bull. **3**(1), 37–46 (1968).
25. J. A. Arnaud, W. M. Hubbard, G. D. Mandeville, B. de la Clavière, E. A. Franke, and J. M. Franke, "Technique for Fast Measurement of Gaussian Laser Beam Parameters," Appl. Opt. **10**(12), 2775–2776 (1971).
26. M. A. de Araújo, R. Silva, E. de Lima, D. P. Pereira, and P. C. de Oliveira, "Measurement of Gaussian laser beam radius using the knife-edge technique: improvement on data analysis," Appl. Opt. **48**(2), 393–396 (2009).
27. M. Jimenez-Rodriguez, L. Monroy, A. Núñez-Cascajero, E. Monroy, M. González-Herráez, and F. B. Naranjo, "Study of Absorption Saturation in InN Thin Films through the Z-Scan Technique at 1.55 μm," in Advanced Photonics 2018 (BGPP, IPR, NP, NOMA, Sensors, Networks, SPPCom, SOF), OSA Technical Digest (online) (Optical Society of America, 2018).
28. S. K. Turitsyn, B. G. Bale, and M. P. Fedoruk, "Dispersion-managed solitons in fibre systems and lasers," Phys. Rep. **521**(4), 135–203 (2012).
29. H. A. Haus, "Theory of mode locking with a slow saturable absorber," IEEE J. Quantum Electron. **11**(9), 736–746 (1975).
30. F. B. Naranjo, M. González-Herráez, S. Valdueza-Felip, H. Fernández, J. Solis, S. Fernández, E. Monroy, J. Grandal, and M. A. Sánchez-García, "Non-linear properties of nitride-based nanostructures for optically controlling the speed of light at 1.5 um," Microelectron. J. **40**(2), 349–352 (2009).